Wear 386–387 (2017) 106–117

Contents lists available at ScienceDirect

Wear

journal homepage: www.elsevier.com/locate/wear

Wear of cemented tungsten carbide percussive drill–bit inserts: Laboratory and field study

Dmitry Tkalich[a,c,*], Alexandre Kane[b], Afaf Saai[b], Vladislav A. Yastrebov[c], Mikko Hokka[d], Veli–Tapani Kuokkala[d], Maria Bengtsson[e], Anna From[f], Carina Oelgardt[g], Charlie C. Li[a]

[a] Norwegian University of Science and Technology (NTNU), Sem Sælands veg 1, NO-7491 Trondheim, Norway
[b] SINTEF Materials and Chemistry, Materials and Nanotechnology, Richard Birkelandsvei 2, NO-7465 Trondheim, Norway
[c] MINES ParisTech, Centre des Matériaux, PSL Research University, CNRS UMR 7633, BP 87, 91003 Evry Cedex, France
[d] Department of Materials Science, Tampere University of Technology, Tampere, Finland
[e] LKAB Wassara AB, P.O. Box 1067, SE-141 22 Huddinge, Sweden
[f] AB Sandvik Mining, Rock Tools, SE-811 81 Sandviken, Sweden
[g] H.C. Starck GmbH, Im Schleeke, D-38642 Goslar, Germany

ARTICLE INFO

Keywords:
Cemented tungsten carbide
Wear
Volume loss
Rotary–percussive drilling
Split Hopkinson pressure bar
Sliding abrasion
Impact abrasion
SEM
Surface deterioration mechanisms
Roughness
Contact area

ABSTRACT

Design of the drill–bit and selection of the Cemented Tungsten Carbide (CC) grade for drill–bit inserts are crucial for efficient percussive drilling. This study presents the results of an experimental campaign executed with the aim to identify the distinctive wear mechanisms and behaviour of different CC grades. Three laboratory and one full–scale drilling tests were performed using nine CC grades with different binder contents, binder chemical compositions, mean tungsten carbide (WC) grain sizes, and grain size distributions. Wear traces found on the drill–bit inserts after the full–scale drilling test show noticeable differences depending on their position on the drill–bit. Tensile forces present on the leading edge of the inserts due to the sliding contact with rock are suspected to play a significant role. Laboratory tests performed include: (i) single impact tests using a modified Split Hopkinson Pressure Bar (SHPB) apparatus, (ii) Abrasion Value (AV) rotating disk tests, and (iii) impact abrasion (LCPC) tests. Volume loss and shape change were used as macroscopic measures of wear. Greater volume losses were found for the grades with nickel–based binders compared to those with pure cobalt binder. The use of a narrower WC grain size distribution leads to lesser volume loss in drilling and AV tests. Surface analysis of the damaged microstructure was performed using scanning electron microscope. Distinct meso–scale (few dozens of WC grain sizes) patterns of damaged microstructure zones surrounded by the intact surface were found on the surfaces of specimens after single impact test. The pattern indicates the potential influence of a non–uniform contact due to the rock roughness and internal rock heterogeneities, which is supported by the study of the rock crater roughness. Size of such zones could be seen as a certain length–scale, which determines the insert–rock contact behaviour. A specific "peeling" mechanism of material removal was observed in the full–scale drilling test, where portion of the CC microstructure fused with the rock tribofilm gets removed when that tribofilm peels off.

1. Introduction

Rotary–percussive drilling (RPD) is a widely–recognized method for mining, tunnelling, and geothermal well applications. The rock breaking during RPD in hard rock formations relies on the rock crushing and chipping mechanisms, achieved by repetitive high speed impacts of a continuously rotating drill–bit [1]. Inserts placed at the head of the drill–bit are the main operating components directly interacting with the rock formation. Their design and wear resistance properties are crucial for rock breaking and tool performance. A composition of a hard ceramic tungsten carbide (WC) and a ductile metallic binder is the most often selected material for drill–bit inserts due to its remarkable wear and fracture resistance [2]. The wear resistance of this composite is usually estimated from its hardness and toughness characteristics together with careful considerations of each particular drilling application, such as the rock type, the environmental, and the operating conditions. However, considering a great number of possible drilling conditions combinations, it would often be a lack of available data on CC behaviour, especially if new types of drilling are employed or new CC grade is being used. Therefore, finding a

* Corresponding author at: Norwegian University of Science and Technology (NTNU), Sem Sælands veg 1, NO-7491 Trondheim, Norway.
E-mail address: dmitrii.tkalich@mines-paristech.fr (D. Tkalich).

http://dx.doi.org/10.1016/j.wear.2017.05.010
Received 10 September 2016; Received in revised form 19 May 2017; Accepted 19 May 2017
Available online 13 June 2017

laboratory test capable of reliably predicting the relative wear resistance of different CC grades is of interest and this issue is addressed in the current study.

Full–scale drilling tests can be performed in order to assess the behaviour of a Cemented Carbide grade but they are highly time and resource consuming. A large tests campaign from single impact tests to full scale fluid hammer tests, to simulate the mining and construction operations, was presented by Konyasahin et al. [3] using CC grades with different binder fractions and mean WC grain sizes.

While the laboratory tests fail to reproduce the full complexity, and coupling of forces acting during real drilling, they can be designed to reproduce some of its major features. The correlations of the CC wear with its hardness and toughness have been highlighted by many investigations (see e.g. [4]), but the question remains regarding the microstructural features' influence. For instance, wear–resistance of different WC–Co grades with similar hardness, varying in both the WC mean grain size and Co content was investigated by Konyasahin et al. [5]; while Angseryd et al. [6] studied the influence of abrasive particles type and size on wear rate. Despite hardness, friability, and size of the abrasive particles, which play a significant role [7,8] the rate of abrasion also depends critically on the CC microstructural characteristics like mean WC grain size, binder mean free path, width of the WC grain size distribution and WC skeleton contiguity [9–11].

In order to get access to the initial stages of the microstructure deterioration processes, appropriate testing procedures should be employed, where the initial degradation traces are not lost. Several examples of such approach can be found in the literature, e.g.: (i) incremental exposure of a CC specimen to a small quantities of erodent [12], and (ii) use of granite and diamond pins to cause localized contacts with CC [13], and (iii) a gradual deterioration of CC microstructure in a sliding wear test [14].

The current study employs a modified Split Hopkinson Pressure Bar (SHPB) apparatus to produce a single impact of a CC drill–bit insert with a rock sample, and capture the initial stages of CC microstructure deterioration. Two complementary abrasion tests were also performed using various CC grades and abrasives of 1–5 mm in diameter created from hard rock formations. In addition, full–scale drilling tests were performed and the results are compared with the laboratory tests' results.

2. Cemented carbide grades

Nine cemented carbide grades were used in the tests. Nominal composition of the tungsten carbide powder and the binder mixtures prior to sintering together with the mechanical properties of the sintered grades are given in Table 1. Grades in Set 1 were used in the single impact tests, whereas the grades in Set 2 were used in the full–scale drilling tests and two laboratory abrasion tests. Grades in Set 1 differ by the WC mean grain size and binder fraction, while those in Set 2 differ in WC grain size distribution and binder composition. The hardness was measured using the Vickers method and the fracture toughness was determined using the Palmqvist method in accordance with the ISO/DIS 28079 standard. Two samples of each CC grade were used with five indentations per sample.

3. Test methods

3.1. Single impact test

High–speed impact interaction of a drill–bit insert and rock was studied using a modified Split Hopkinson Pressure Bar (SHPB) testing apparatus. Transmitted bar in the original configuration was replaced by a fixed block of Kuru grey granite rock (30 × 30 × 30 cm^3), which served as the target, while the intact CC insert was fixed at the end of the incident bar facing the rock block, as illustrated in Fig. 2(a). Surface of the rock block at the place of impact was finely polished. During the test the striker bar is impacted at the free end of the incident bar at a speed of 11 m/s generating a stress wave propagating in the bar towards the end with a CC insert and the rock specimen. As the stress wave reaches the CC insert, a part of the stress wave is reflected back to the incident bar as a wave of tension, and part is transmitted into the rock causing dynamic impact damage on the rock and on the CC insert. The stress wave reflected back into the incident bar travels back and forth resulting in a succession of attenuated rebounds. High–speed camera images of the impact are shown in Fig. 2(b). Three inserts of each grade from Set 1 were tested.

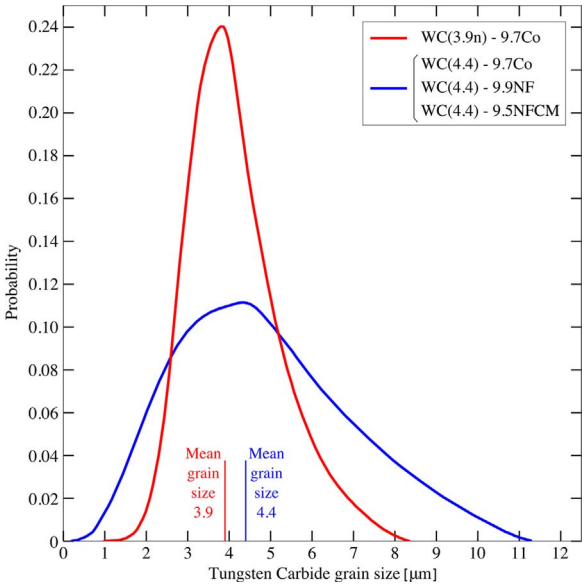

Fig. 1. WC grain size distribution for grades in Set 2.

3.2. Full–scale drilling test

Full–scale drilling (FSD) tests are performed using drill–bits of conventional size and geometry, as shown in Fig. 3(a). FSD tests were performed at underground Malmberget mine (municipality of Gällivare, Sweden) with an average rotation speed of 80 rev/min, feed force of 4.3kN, and percussion frequency of 65 Hz. Drilling paths of average length of 80 m passed predominantly through the Red Leptite rock formation with an intact strength of 184 MPa [15]. X–ray diffraction analysis of the Red Leptite's powder from the drilling site revealed the following mineral composition: 45.68% Albite, 23.83% Microcline maximum, 14.17% Quartz, 7.22% Diopside, Hornblende 5.6%, and 3.5% other.

Each drill–bit was equipped with CC inserts of identical grade, as shown in Fig. 3(b). One drill–bit for each one of four CC grades in Set 2 was tested. Inserts placed at the outer bevelled edge (positions numbered 1–10) are referred to as "peripheral inserts" and those on the flat frontal plateau (positions numbered 11–19) as "face inserts".

3.3. Sliding abrasion test

In the Abrasion Value (AV) test [16], a CC specimen is abraded by loose crushed rock particles distributed over a rotating disk surface, as illustrated in Fig. 4. Dead weight of 10 kg is used to press the specimen against the disk, which rotates at the speed of 20 rev/min. Resulting linear velocity of the specimen hitting the rock particles on the disk is of 0.35 m/s. The crushed rock is continuously renewed after it passes beneath the CC specimen. Weight loss of the specimen is measured after 5 min of testing when it travelled 100 m over the abrasive disk.

The crushed rock used in this test was Kuru grey granite (quarried in Kuru, Finland), with the density of 2630 kg/m^3 and mineral grain sizes

Table 1
Nominal composition and structural characteristics of the investigated Cemented Carbide grades.

	Grade designation[a]	Raw materials (prior sintering)			Sintered Cemented Carbide		
		Binder (vol %)	Binder composition (wt%)	Mean WC grain size [μm]	Vickers Hardness [Hv20][c]	Density [g/cm^3]	Fracture toughness (KIc) [MPa √m][c]
Set 1	WC(2.0)–22.9Co	22.9	Co 100%	2	1150 ± 4.5		
	WC(2.5)–9.7Co	9.7		2.5	1400 ± 2		
	WC(3.5)–16.6Co	16.6		3.5	1220 ± 3.5		
	WC(5.0)–9.7Co	9.7		5	1270 ± 3		
	WC(7.5)–9.7Co	9.7		7.5	1190 ± 3		
Set 2	WC(3.9n)–9.7Co	9.7	Co 100%	3.9[b]	1461 ± 3	14.98	11.1 ± 0.3
	WC(4.4)–9.7Co	9.7	Co 100%	4.4[b]	1465 ± 3	14.97	10.8 ± 0.1
	WC(4.4)–9.9NF	9.9	Ni 85% Fe 15%	4.4[b]	1423 ± 2	15.00	10.4 ± 0.1
	WC(4.4)–9.5NFCM	9.5	Ni 39.4% Fe 39.4% Co 19.7% Mo 1.5%	4.4[b]	1448 ± 3	14.92	9.0 ± 0.1

[a] Designations are constructed as follows: WC(*X*) – *Y Z*, where *X* is the mean WC grain size, *Y* is the binder vol% and *Z* is the binder composition. Marking "*n*" in WC(3.9n)–9.7Co stands for a narrower WC grain size distribution, compared to other grades in Set 2.
[b] WC grain size distribution curves are shown in Fig. 1.
[c] Mean value and the 95% confidence interval are given.

varying from 0.5 to 1.5 mm. The mineral composition of the rock obtained by X–ray diffraction analysis is the following: 35.3% Quartz, 30.4% Albite intermediate, 28% Microcline, and 6.3% other. Uniaxial compressive strength of Kuru granite is 236 MPa and Vickers hardness is 850HV [17]. In accordance with the preparation procedure given by Dahl et al. [18] the rock was crushed to powder, where 99% of granular rock are < 1 mm in diameter and 70 ± 5% are < 0.5 mm.

3.4. Impact abrasion test

"LCPC" abrasion test was originally developed at the Laboratoire Central des Ponts et Chaussées to study rock and soil abrasivity (Normalisation Française P18–579). The rectangular metal impeller rotates in a cylindrical container with rock particles. The measure of the rock sample abrasivity is the mass loss of the impeller during the test. For the current study the LCPC test setup was kept in its original form, but with a metal impeller adapted to hold two rectangular parallelepiped CC specimens, as illustrated in Fig. 5. The mass loss of the specimens was used to characterize the CC grade performance, rather than the abrasivity of rock. Impeller rotates at a speed of 4500 rev/min, resulting in a mean linear velocity at which the specimens hit rock particles of 6.7 m/s. The rock used in this test was Kuru grey granite. In accordance with the preparation procedure for the LCPC test, the rock was crushed to particles of 4–6.3 mm in diameter and renewed for each test. By the end of the test rock particles' size were reduced to about

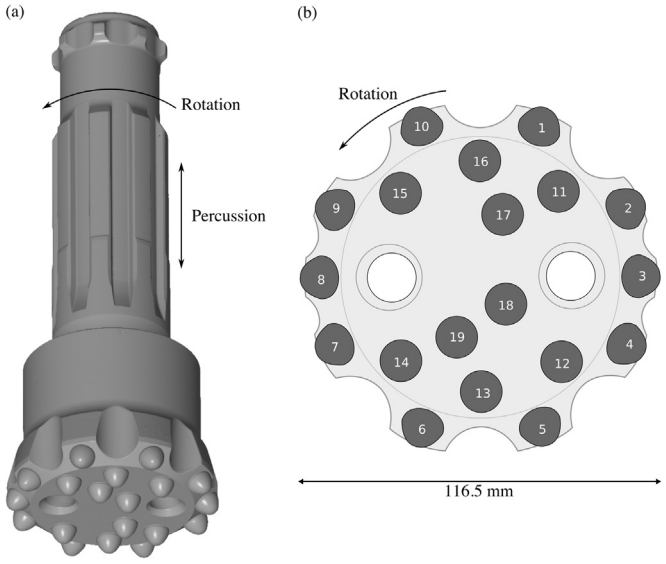

Fig. 3. (a) Drill–bit used in the full–sale field drilling tests. (b) Frontal view of the drill–bit crown equipped with 19 parabolic spherical–tipped cemented tungsten carbide inserts (in dark grey).

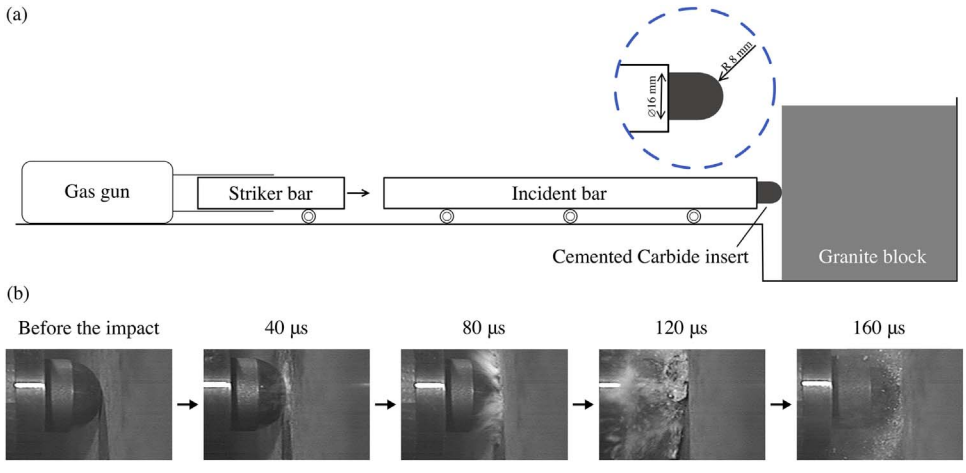

Fig. 2. (a) A schematic illustration of the modified Split Hopkinson Pressure Bar testing apparatus and (b) high–speed camera photos of the insert–rock impact at 40μs intervals.

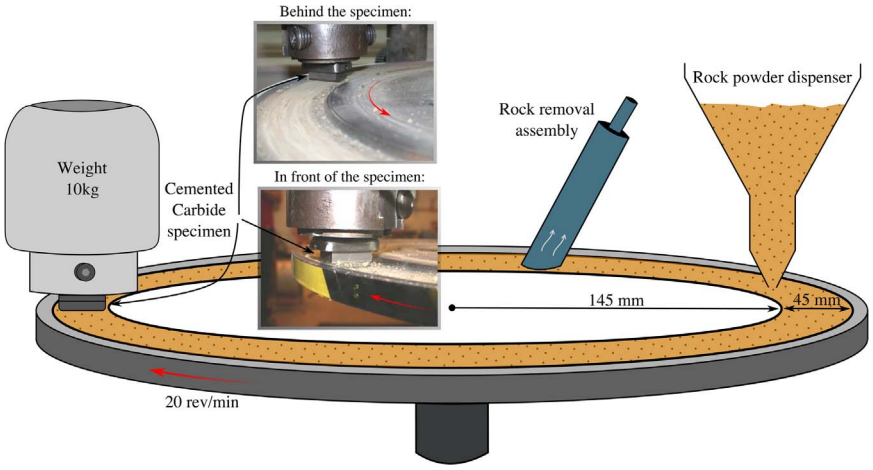

Fig. 4. Schematic illustration of the sliding abrasion AV test.

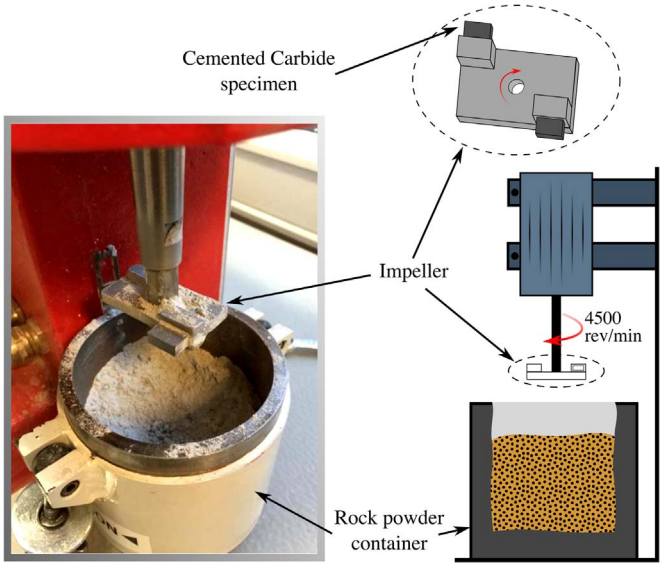

Fig. 5. Schematic illustration of the impact abrasion LCPC test with a metal impeller adapted to hold two rectangular parallelepiped CC specimens. On the photo the impeller is lifted from the rock container.

0.5 mm in diameter. Weight loss of the CC specimens was measured after five minutes of testing, when the specimen had travelled 24 km.

4. Results and discussion

After the tests, the inserts form the SHPB and the FSD tests and the specimens from AV and LCPC tests were cleaned in acetone using an ultrasonic washer. Examination in the scanning electron microscope (SEM) was performed using both the secondary electron (SE) and the backscatter electron (BS) detectors at accelerating voltages 10, 15, 20 and 29 kV and probe current of 80–100 nA. When available, a 70% transparent BS image was overlaid on top of the SE image to combine morphology and chemical composition information. In addition, the colour spectrum of the initially grayscale BS image was adjusted towards brown spectrum, making the light–grey WC grains and binder of brown hue, while the black rock – of light grey hue.

4.1. Actual insert–rock contact area

A single insert–rock impact test was performed using a modified SHPB apparatus with the aim of studying the initial stages of the interaction process. Mild damage of the CC insert's surface from a single impact to an intact rock surface allows to draw more distinct conclusions on the degradation mechanisms involved than from the specimens observed after the wear–steady state tests carried out in this study.

Damaged insert surfaces of each grade from the Set 1 show distinct patterns of zones of damaged microstructure surrounded by intact surface, when examined in SEM. Zones of damaged microstructure vary in size from 20 to 250 μm in diameter. Various CC inherent microstructure deterioration mechanisms can be found within those zones: binder extrusion, slip–bands and cracks in the WC grains, removal of WC fragments and whole grains, penetration of rock material into the appeared cavities. Several SEM images are shown in Fig. 6 illustrating the abovementioned non–uniform damage patterns at different magnifications. Black– and grey–coloured patches on the surface are the adhered rock material marking the zones of insert–rock contact. The degree of CC microstructure damage gradually decreases with the distance from the centre of those damaged zones. Fig. 6(b.4) shows a close up of an edge of one damaged zone where cracked WC grains, depleted binder, and the remained intact surface at the bottom left corner of the picture are visible. Shape of the damaged zones, best seen in Fig. 6(a.3), (a.4) and (b.3) can be characterized by consisting of a main pit of impact and trails of a milder damage areas produced most likely by the rock asperities crushed during the impact. Such milder damage trails can be seen in Fig. 6(a.3) directed from the left to the right side of the image, in Fig. 6(a.4) from top to bottom, and in Fig. 6(b.3) from top right to bottom left.

The observed patterns indicate the non–uniform nature of the contact due to the rock roughness and internal rock heterogeneities. Such non–uniform contact took place despite the fact that surface of the rock used in the impact tests was finely polished, which suggests that the interaction with a crushed rock surface would certainly lead to a highly irregular pattern of contact zones.

The craters caused by the impact on the rock surface were analysed using a 3D optical profilometer with a resolution of 0.05 μm in the vertical direction and 6.9 μm in the two in–plane directions. The 3D reconstruction of one of the craters is shown in Fig. 7(a). The potential pattern of contact zones in the subsequent impacts could be estimated from the profile. Contact zones are obtained by intersecting the digital replica of the crater with a virtual surface resembling the shape of a spherical tip of the CC insert. No deformation of the insert or the rock is taken into account during this virtual penetration. The simulated pattern of contact zones is shown in Fig. 7(b) and (c) at various depths of insert's penetration and qualitatively resembles those observed on the inserts' damaged surfaces illustrated in Fig. 6(a.1) and (b.1). This confirms the potential correlation of the rock's surface roughness and underlying heterogeneity with the irregular pattern of damaged zones found on CC inserts' surfaces.

Size of the insert–rock contact zone could be seen as a certain

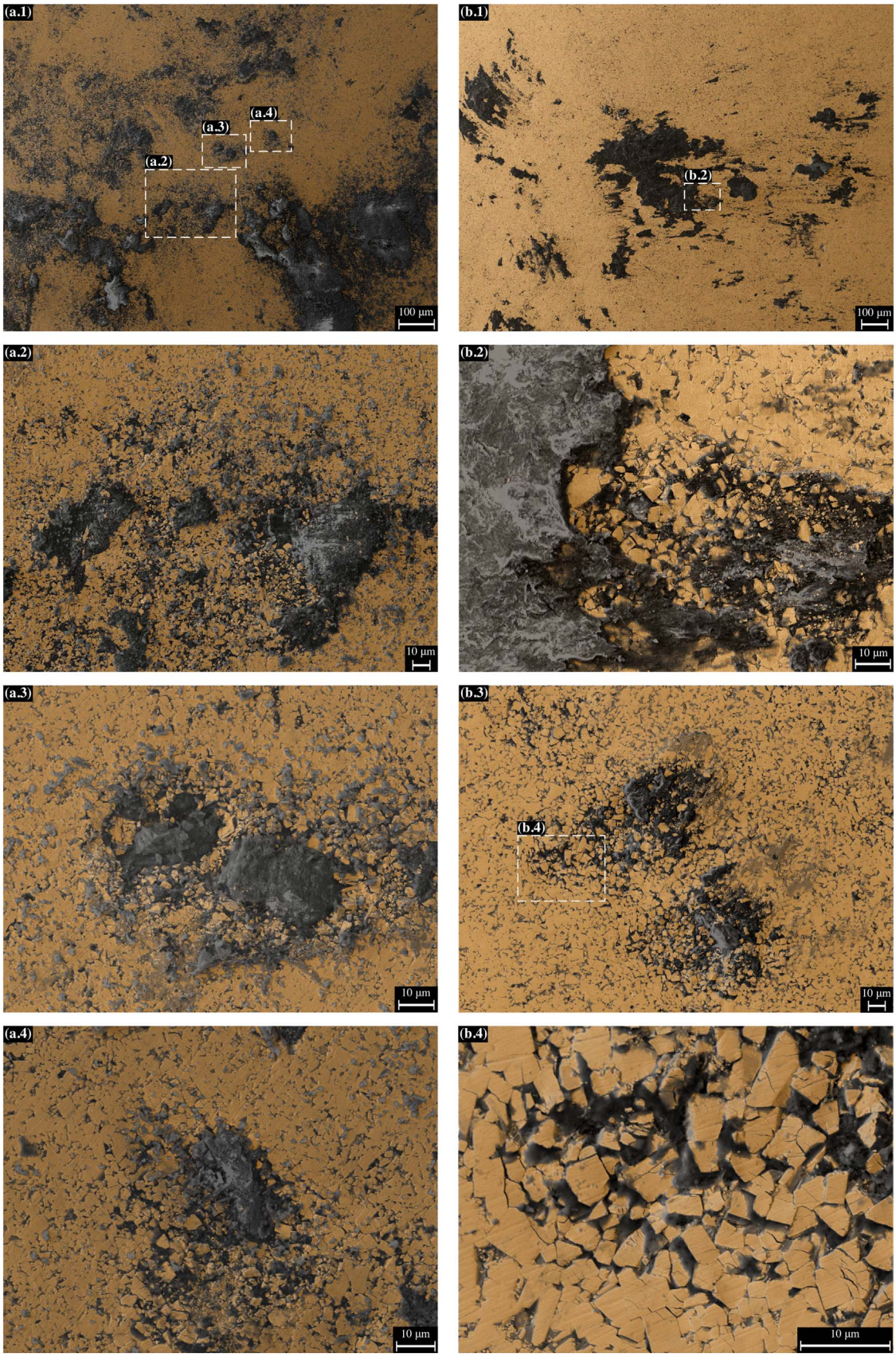

Fig. 6. SEM images (SE and BS images overlaid) of the CC insert's surfaces after the single impact SHPB test at different magnifications, where zones of damaged microstructure are found to be surrounded by intact surface. (a) WC(2.5)–9.7Co grade (b) WC(3.5)–16.6Co. Electron accelerating voltage of 10 kV was used to obtain SEM images.

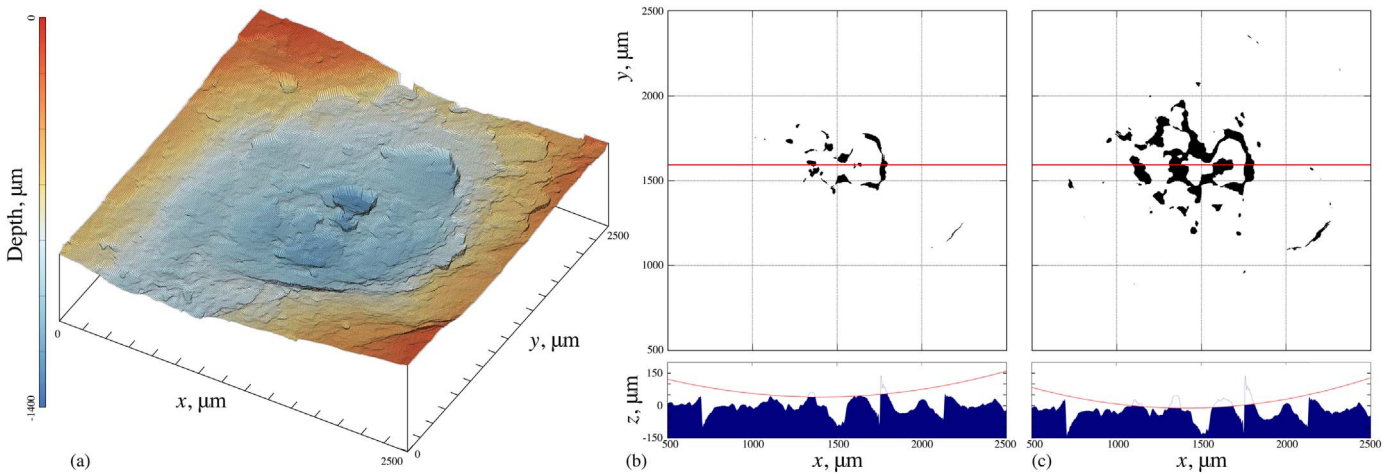

Fig. 7. (a) 3D reconstruction of a crater in Kuru grey granite produced by a single impact SHPB test. (b) Potential pattern of contact zones estimated by intersecting the digital replica of the crater with a virtual surface resembling the shape of a spherical tip of the CC insert.

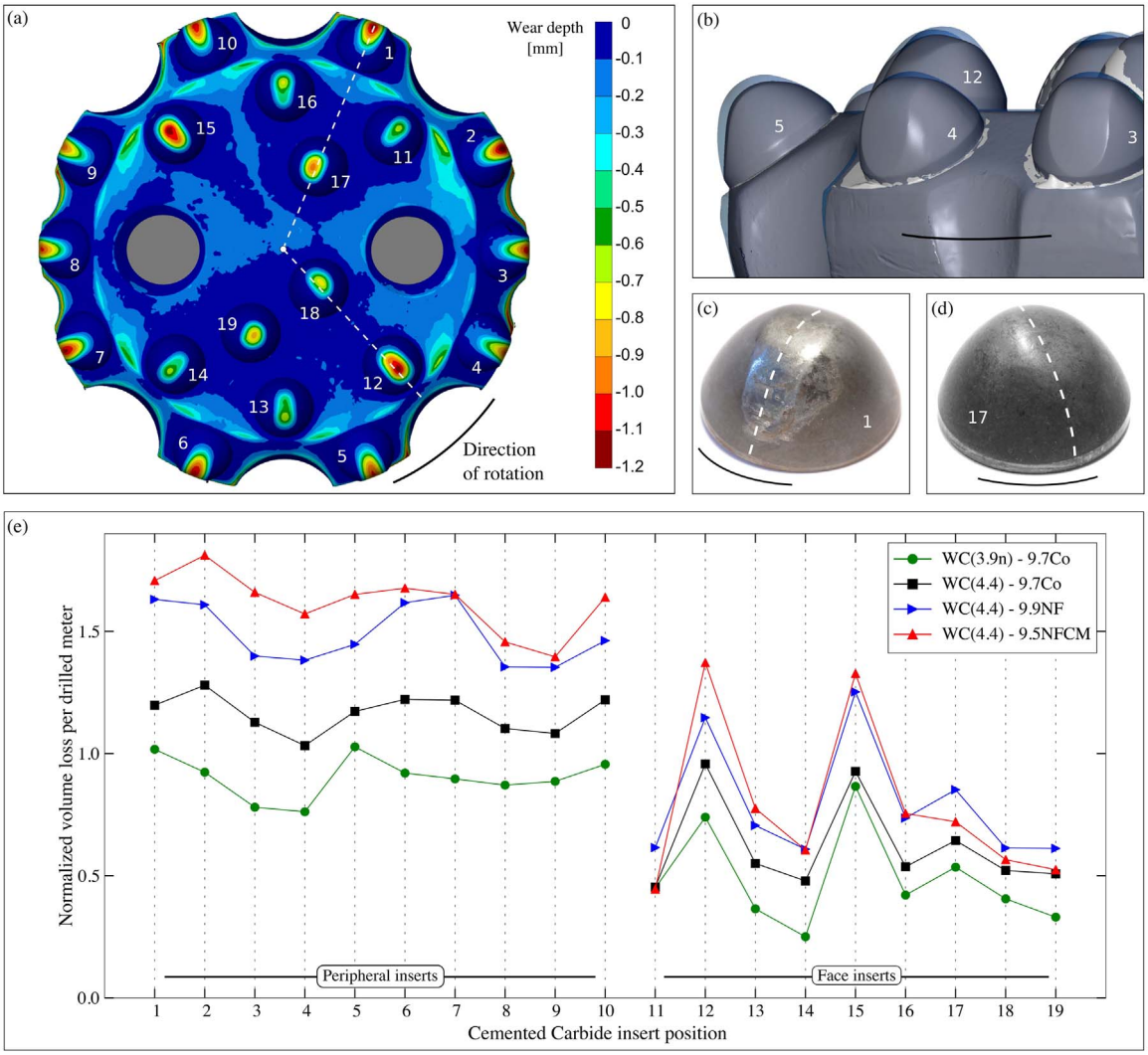

Fig. 8. (a) Material loss map generated by GOM software for the drill–bit equipped with WC(4.4)–9.5NFCM grade inserts in frontal view. White numbers give the reference position of each CC insert. (b) Initial(transparent) and worn(solid) shape comparison with a zoom to peripheral inserts in positions 3, 4 and 5. Worn insert (c) in position 1 (d) in position 17, with dash white line showing the radial direction, as shown in (a). (e) Volume loss per drilled meter for each insert on the drill–bit normalized by the mean volume loss over all inserts of the same grade.

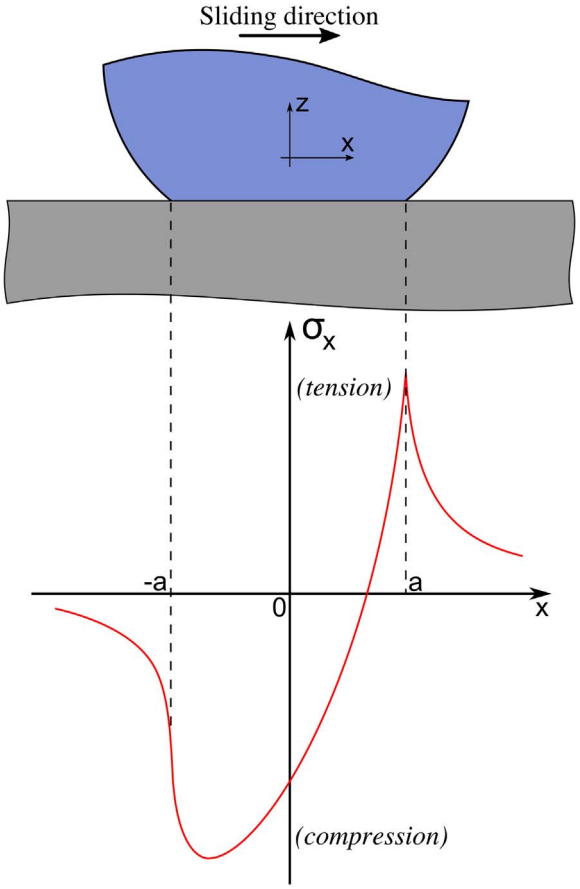

Fig. 9. Distribution of in–plane σ_x stress along the surface of the upper body in a circular frictional sliding contact [24]. Tensile part of σ_x is the largest acting on the surface.

Table 2
Average volume losses in the FSD tests for each CC grades from Set 1.

Grade	Average volume loss per drilled meter [mm^3]		
	All inserts	Face inserts	Peripheral inserts
WC(3.9n)–9.7Co	0.414	0.284	0.530
WC(4.4)–9.7Co	0.532	0.364	0.684
WC(4.4)–9.9NF	0.681	0.466	0.874
WC(4.4)–9.5NFCM	0.720	0.462	0.952

characteristic length–scale of the interaction. The behaviour of the CC at this scale would determine the overall response and wear of the insert. Several studies have been carried out in this direction. The relationship between the microstructural scale of the composite and of the local contact conditions was highlighted by Nabarro et al. [19] and Shrivatsava et al. [20], who performed tests using WC–Co micro–indenters of various sizes. Conrad et al. [21] and Anand and Conrad [22] investigated the response of WC–Co to the impacts of particles of different sizes. The studies showed that when a crater created after an impact of alumina particles affects an area less than 10 WC grains, the material degrades mainly by brittle fracture of the WC grains, but when the impact area covers more than 100 WC grains, the deterioration is governed mainly by plastic deformation and ductile fracture of the binder phase.

4.2. Wear of CC inserts in full–scale drilling test

Measurements of the drill–bit wear in FSD tests were made using GOM optical measuring system [23]. Shape of each drill–bit is recorded before and after the drilling test in a form of 3D cloud of points, which

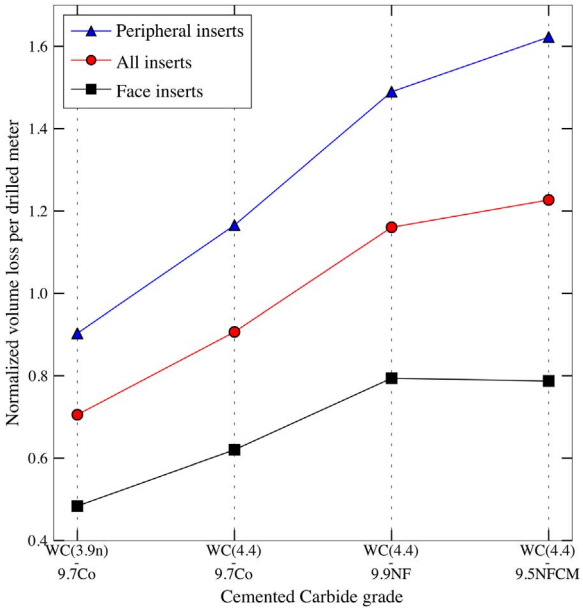

Fig. 10. Average volume losses in the FSD tests for each CC grade from Set 1.

allows shape comparison and volume difference calculation. Material loss map generated using the GOM Inspect software is shown in Fig. 8 for the drill–bit equipped with WC(4.4)–9.5NFCM grade inserts. Macroscopic wear patterns for the inserts in the same position on the drill–bit do not differ for different CC grades, thus the wear pattern discussed in this section is common for all grades in Set 2. Only an analysis of the CC inserts' material loss is considered here, the drill–bit steel crown wear is not discussed and not included in calculations.

Wear traces differ in shape and size on the peripheral and face inserts, as shown in Fig. 8(c) and (d), respectively. The comparison of the initial and the worn shapes is illustrated in Fig. 8(b) with a zoom to the inserts in positions 3, 4, and 5. Wide flat wear traces are pronounced on the sides of peripheral inserts facing borehole wall and elongated along the borehole axis. The glossy appearance of the worn surface in Fig. 8(c) is due to the rock tribofilm layer, which is examined in Section 4.5. Also, a less pronounced, but noticeable wear trace (also covered with tribofilm) is found on the leading edge of the peripheral insert with respect to the direction of drill–bit rotation (see in Fig. 8(c)). Thickness of the tribofilm does not exceed 30 μm, which is insignificant for the macroscopic wear pattern analysis.

Considering the relative position of the inserts on the periphery with respect to the direction of rotation, one can see that inserts in positions 3 and 4 could be seen as being protected by the insert in position 2, similarly for the positions 8 and 9 being protected by 7. That can be explained by the positions 2 and 7 being leading with respect to the direction of drill–bit rotation and by the considerably smaller sockets designed between positions 2 and 3, 3 and 4, 7 and 8, 8 and 9. The sockets serve as pathways for rock debris removal from the bottom of the hole by ascending along the borehole walls. Measurements of volume losses for each insert separately, shown in Fig. 8(e), confirm that the inserts in positions 3 and 4 exhibit less volume loss compared to the one in position 2 and similarly for the inserts in positions 8 and 9 compared to the one in position 7. It could be expected that volume loss for the inserts in positions 1, 2, 5, 6, 7 and 10 would be similar and higher than for other peripheral inserts. It is roughly true; however, some discrepancy remains since the set of data is not statistically significant.

For the face inserts two domains could be distinguished which differ by the shape of the wear traces. The first domain consists of inserts placed near the edge of the face plateau – in positions 11–16, the second domain consists of inserts closer to the centre of the face plateau – in

Table 3
Volume losses in sliding abrasion AV and impact abrasion LCPC test. Measurements marked with "(c)" correspond to cases where chipping of the specimen's corner was evident and are not taken into account in average calculations.

Grade	Volume loss in AV test [× 10^{-2}%]					Volume loss in LCPC test [× 10^{-2}%]				
	Average	Test 1	Test 2	Test 3	Test 4	Average	Test 1	Test 2	Test 3	Test 4
WC(3.9n)–9.7Co	3.04	2.97	3.12	–	–	6.85	6.85	6.85	6.85	17.97(c)
WC(4.4)–9.7Co	3.41	3.41	3.41	–	–	5.35	5.99	5.14	5.99	4.28
WC(4.4)–9.9NF	3.19	3.26	3.56	3.11	2.81	10.26	11.97	8.55	10.26	31.62(c)
WC(4.4)–9.5NFCM	4.51	4.77	4.02	4.62	4.62	10.60	11.17	9.45	11.17	18.04(c)

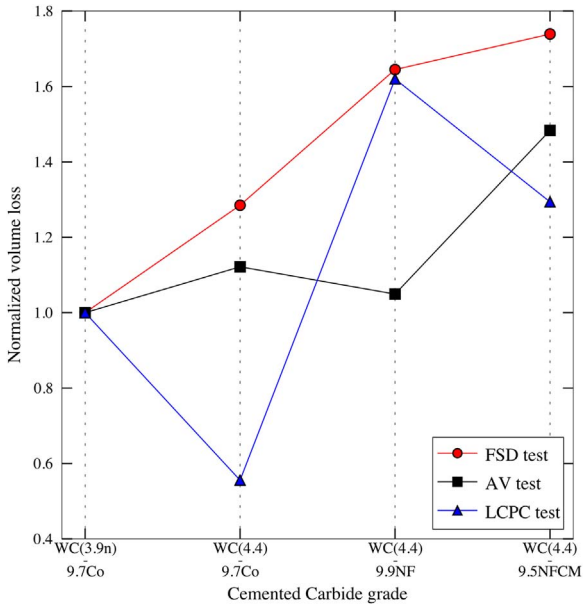

Fig. 11. The comparison of the normalized volume losses in full–scale drilling, sliding abrasion AV test, and impact abrasion LCPC test. For each test the measurements are normalized by that for the grade WC(3.9n) –9.7Co in the test.

positions 17–19. Wear traces on the insets in the first domain are elongated along drill–bit's radial direction and inclined towards the insert's leading edge. Within this domain, the inserts in positions 12 and 15 show significantly higher volume losses, as shown in Fig. 8(e). Excessive material loss of these two inserts, compared to the inserts in positions 11, 13, 14 and 16, can be explained by their leading position with respect to the direction of drill–bit rotation and thus being more exposed to the intact rock than the latter, as can be seen in Fig. 8(a). Volume loss for the inserts in positions 12 and 15 is similar to that exhibit by the peripheral inserts, as shown in Fig. 8(e), which, considering the difference in the travel distance and linear velocity, signifies of their dangerous position.

Wear traces on the inserts in the second domain of face inserts have circular shapes and inclined form the tip in the direction of drill–bit rotation, as shown in Fig. 8(a) and (d) for the inserts in positions 17, 18 and 19. The insert in the position 18 exhibits the lowest linear velocity and the shortest travel distance among all the inserts. However, its volume loss is not the lowest, but higher than those from the "protected" face inserts in positions 11, 13, 14, and 16. That perhaps can be explained by it being the only one which does not have the symmetrically placed insert – see the empty space in Fig. 8(a) between one nozzle and inserts in positions 15, 17 and 18.

The inclination of all the wear traces towards the insert's leading edge can be explained by the harmful tensile forces present on this edge of the insert due to the sliding contact with rock [24], as illustrated in Fig. 9. Numerical investigation of the significant effect of such tensile forces on the CC microstructure behaviour can be found in [25]. The change in wear traces' shape from circular to elliptical towards the drill–bit periphery might be attributed to the difference in linear speed for the inserts in different position and thus the difference the induced tensile force magnitudes.

Average volume losses for each CC grade are given in Table 2 and shown in Fig. 10. General tendency for all CC grades is that volume loss on the peripheral inserts is about 1.9 times higher than that for the face inserts of the same grade. Grade WC(3.9 n)–9.7Co with a narrower WC grain size distribution exhibit lower volume loss compared to that for the grade WC(4.4)–9.7Co with a wider WC grain size distribution, while both grades have same binder composition and fraction. Increase in volume loss for these two grades differs only by 0.8% between peripheral and face inserts, being greater for the former. Binder composition also significantly affects the wear resistance. Grade with pure Cobalt binder exhibits the lowest volume loss among the three, followed by the grade with binder consisting of 85% Nickel and 15% Iron, while the one with binder consisting of 39.4% Nickel, 39.4% Iron, 19.7% Cobalt and 1.5% Molybdenum exhibiting the highest volume loss. Difference in volume loss between the latter two is less pronounced compared to the former pair. The wear of peripheral inserts is more influenced by the binder composition compared to the face inserts.

The wear of CC inserts in drilling was often classified as being of an abrasive type. However, in the study by Swick et al. [26] no signs of abrasive wear scratches were found on the inserts used in rotary–percussive drilling. Explanation to such observation could be found in the work by Bowden and Tabor [27], where material loss in sliding abrasion tests was investigated. This study concludes that, irrespective of hardness of the two interacting bodies, the one with lower melting temperature will be abraded and will lose the most weight. In the case of the FSD test, hardness of quartz is of the same order as the hardness of the CC, however, the melting temperature of the latter is 1.7 times higher than that of the former. Confirmation of the non–abrasive nature of CC wear can be found in Section 4.4, where SEM images of the worn surfaces are shown, demonstrating no signs of abrasive wear scratches.

4.3. Laboratory abrasion tests

The volume losses in percentage to the total volume of the specimen are presented in Table 3 for sliding abrasion AV and impact abrasion LCPC tests for each CC grade in Set 1. Volume losses were calculated from weight change measurements. The average results were calculated from two or four tests for the AV test and from three or four tests for LCPC test. Three specimens exhibited noticeable chipping during LCPC test, these results are marked with "(c)" in Table 3 and are not taken into account in the calculations of the average volume losses.

The comparison of the normalized volume losses in FSD, AV, and LCPC tests is shown in Fig. 11, where the grade WC(3.9n)–9.7Co is selected as the reference to compare the relative wear resistances of different grades. The rock type used in the AV and LCPC tests differs from the one in the full–scale drilling. Nevertheless, both Kuru granite and Malmberget Red Leptite can be qualified as hard brittle rocks of Class II [28] which allows to make qualitative comparison of the wear induced on CC specimens and inserts.

The comparison of the volume losses for the grades WC(3.9n)–9.7Co and WC(4.4)–9.7Co show the influence of the initial WC grain size

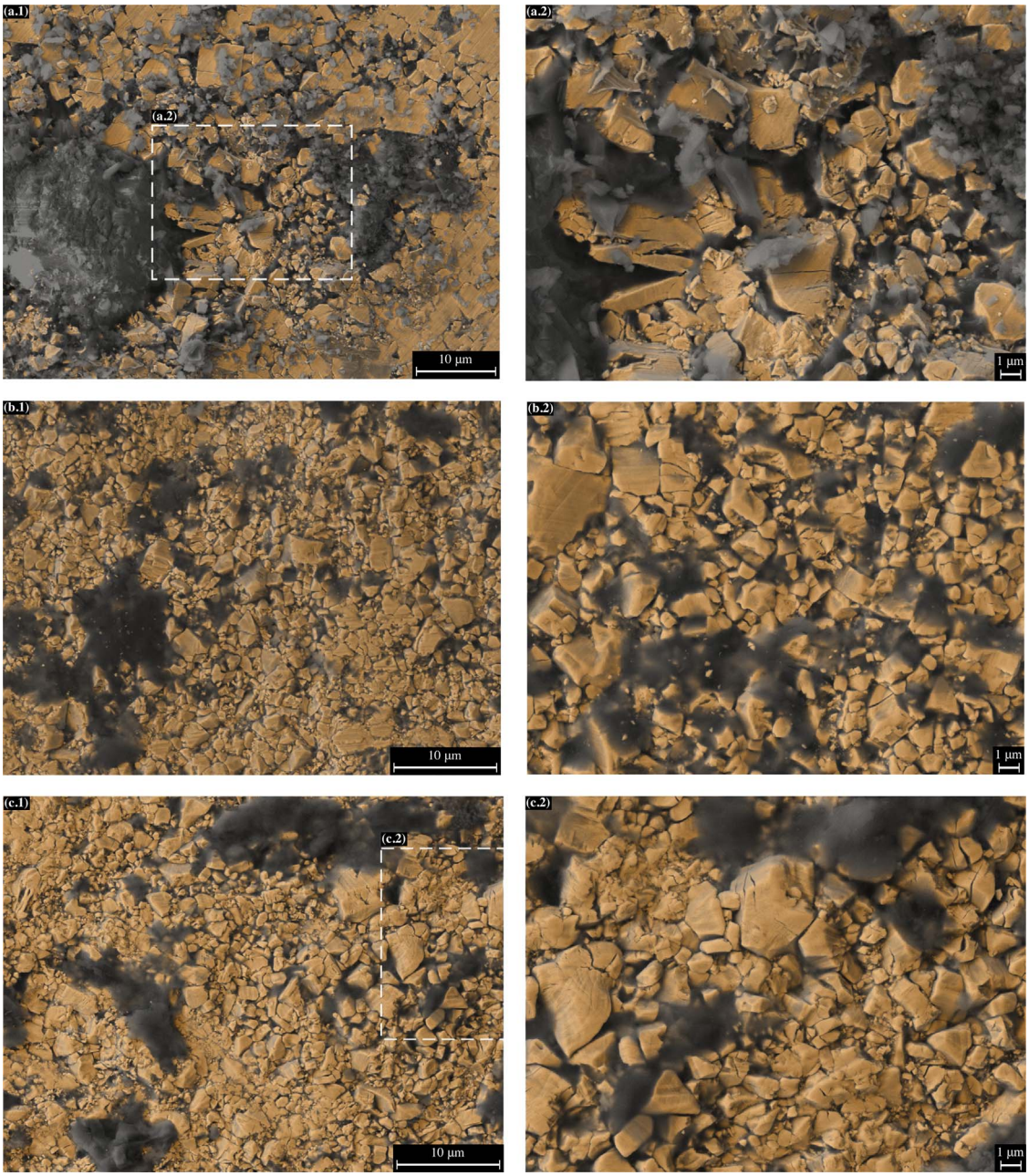

Fig. 12. SEM images (SE and BS images overlaid) of the worn surface of the (a) CC insert WC(2.5)–9.7Co from the SHPB test and WC(4.4)–9.5NFCM specimens from (b) AV and (c) LCPC tests. Electron accelerating voltage of 10 kV was used to obtain SEM images in (a) and 15 kV – in (b) and (c).

distribution of raw WC powders. The AV test results show higher wear resistance with a narrower WC distribution, which is consistent with the result of the FSD test; while the LCPC test gives the opposite tendency: the volume loss for the WC(3.9n)–9.7Co grade is almost twice higher than that of the WC(4.4)–9.7Co grade.

The influence of the binder composition on the wear resistance can be deduced from the test results of the grades WC(4.4)–9.7Co, WC(4.4)–9.9NF, and WC(4.4)–9.5NFCM. It appears that the wear resistance varies with the type of tests performed. For the first pair of grades the tendency in wear resistance change observed in the LCPC test is consistent with that obtained in the FSD test, while the AV test gives the opposite result. For the latter pair the AV test results are consistent with the FSD results, while the LCPC test result shows the opposite trend. For the pair WC(4.4)–9.7Co and WC(4.4)–9.5NFCM all tests agree in a prediction of higher volume loss for the latter.

Overall it can be concluded that it remains challenging to obtain from the laboratory abrasion tests a reliable and conclusive predictions regarding the relative performance of CC grades in drilling. Some tendencies in wear resistance change are captured correctly, but the tests lack the accuracy in predicting the relative magnitudes of volume losses. This inconsistency can be explained by the fact that temperature, stress and lubrication conditions differ in all three tests. However, the AV test seems to be more reliable in predicting the relative CC grade volume loss, which can be attributed to the similarity of linear speed of the interaction with rock. Speed of 0.35 m/sec in AV test is similar to that for the CC inserts in the FSD test, where speeds are ranging from 0.08 to 0.44 m/sec, depending on the insert position. In LCPC test both the specimen geometry and the abrasive action differ considerable from those of the full–scale drilling. In perspective, using a rounded specimen geometry and lower rotation speed should be considered for the LCPC test.

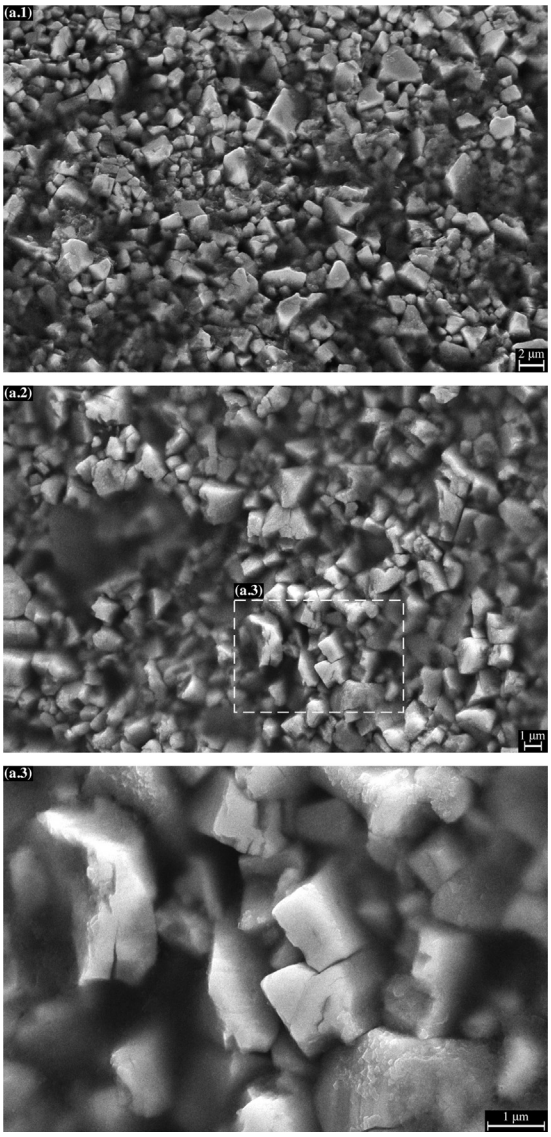

Fig. 13. SEM SE images of the worn surface of the CC insert WC(4.4)–9.7Co in position 17 (face insert) after FSD test. Electron accelerating voltage of 29 kV was used.

4.4. Micro–mechanisms of surface deterioration

SEM images of the worn surfaces of the CC inserts from the SHPB test and specimens from the AV and LCPC tests are shown in Fig. 12(a), (b) and (c), respectively. Microscopic deterioration mechanisms observed on the damaged surfaces of all the CC grades are in line with many studies of the wear of the CC materials [4,29,30]. The following types of degradation mechanisms can be distinguished in Fig. 12:(i) plastic deformation and extrusion of the binder and binder/rock mixture, (ii) plastic deformation and cracking of the WC grains and release of fragments, (iii) detachment of whole or parts of the WC grains. Appearance of the worn surfaces shown in Fig. 12 are representative of that for all the CC grades used in the corresponding test. Despite the difference in the test conditions the appearance of the worn surfaces after AV and LCPC tests is strongly similar showing WC grains with rounded edges and small fragments of WC grains fused with the rock tribofilm filling the spaces between larger grains. That results in a rather levelled topology, compared to the WC grain size. Surface damage after the single impact SHPB test in Fig. 12(a) seems to be more severe, compared to that after the AV and LCPC tests, however, this impression is misleading. The damaged zone in Fig. 12(a.1) is created by the localized interaction with the rock due to its roughness, as discussed in Section 4.1 and illustrated in Fig. 6. Most of the surface of the insert is intact and thus an average damage level is significantly lower than that after the AV and LCPC tests.

Certain differences could also be found between the CC worn surfaces after FSD test and those after the AV and LCPC tests. Example of a worn surface of the WC(4.4)–9.7Co CC insert in position 17 (face insert) is shown in Fig. 13. High accelerating voltage of 29 kV is used to look past the rock tribofilm covering most of the surface. The first to be noticed is that the WC grains are not rounded, but rather sharp-edged, and also the size of the grains (1.5 μm) appears to be smaller than the 4.4 μm for the nominal composition. Second, the surface topology does look levelled, but only owing to the rock tribofilm filling the pits in the microstructure. The amount of rock tribofilm covering the surface is substantially greater than that in the laboratory tests and it is especially the case for the inserts in a peripheral position, which are analysed in Section 4.5. One similarity between all the test is that no abrasive wear scratches were found in either of the tests (see Figs. 12 and 13). This supports the reasoning given in Section 4.2 regarding the non–abrasive nature of CC microstructure deterioration when in contact with rock. Another important aspect for the CC microstructure deterioration is the presence of tensile stresses on the leading edge of the insert due to the frictional sliding contact with rock, as illustrated in Fig. 9. Cemented Carbides' lower strength in tension facilitates wear of the leading edge of the sliding CC insert or specimen by means of WC grain cracking. However, no large presence of cracked WC grain is found on the worn surfaces after either AV or FSD tests, as shown in Figs. 12(b) and 13, respectively. This could be explained by the meso–scale size (several dozens of WC grains) of the area of induced tensile stresses, rather than their localized appearance. Conditions of the impact abrasion LCPC test do not promote sliding contact and such tensile stresses shouldn't be expected to occur. Worn CC surface after LCPC test show no large presence of cracked WC grain, as shown in Fig. 12(c). Overall it can be concluded that the response and appearance of the CC microstructure in laboratory test is similar to that in the full–scale drilling, however the appearance differ by the amount of rock tribofilm on the surface and by the rounded versus angular shapes of WC grains.

4.5. Peeling mechanism of material removal

Surface of the peripheral inserts after the FSD test differs from that observed for the face inserts. As illustrated in Fig. 8(a–c), the peripheral inserts predominantly lose material form the side facing the borehole wall. The SEM investigation shows that this side is covered by a rock tribofilm with a thickness of about 30 μm, as shown in Fig. 14. The evidence of dominating tangential forces can be clearly seen on the surface of the rock tribofilm in Fig. 14(a.2–3) and (b.2) as morphological relief and scratches oriented parallel to the direction of drill–bit rotation. This suggests that the tribofilm forms gradually during drilling by adhesive layup of the crushed rock material mixed with extruded CC binder and broken off pieces of WC grains.

Patches of naked CC surface surrounded by the tribofilm, as shown in Fig. 14(a.2) and (a.3), and sharp ripped–off–like edges of tribofilm, as shown in Fig. 14(b.1) and (b.2), both suggests that eventual tribofilm removal occurs incrementally through peeling off patches of 50–200 μm in diameter. Fig. 14(a.4) shows a partly peeled–off tribofilm patch, where also pieces of WC grains are visible as light grey inclusions within the tribofilm bulk. The CC microstructure underneath those peeled–off patches shows no presence of cracks or slip–bands in the WC grains and no traces of either binder or rock, as shown in the bottom left part of the Fig. 14(b.4). This suggests that the microstructure was initially protected by the tribofilm. When the tribofilm gets peeled off, a portion of the CC microstructure, which was fused with the tribofilm, gets removed as well. That leaves an exposed, undamaged and binder–less appearance of the underlying layer.

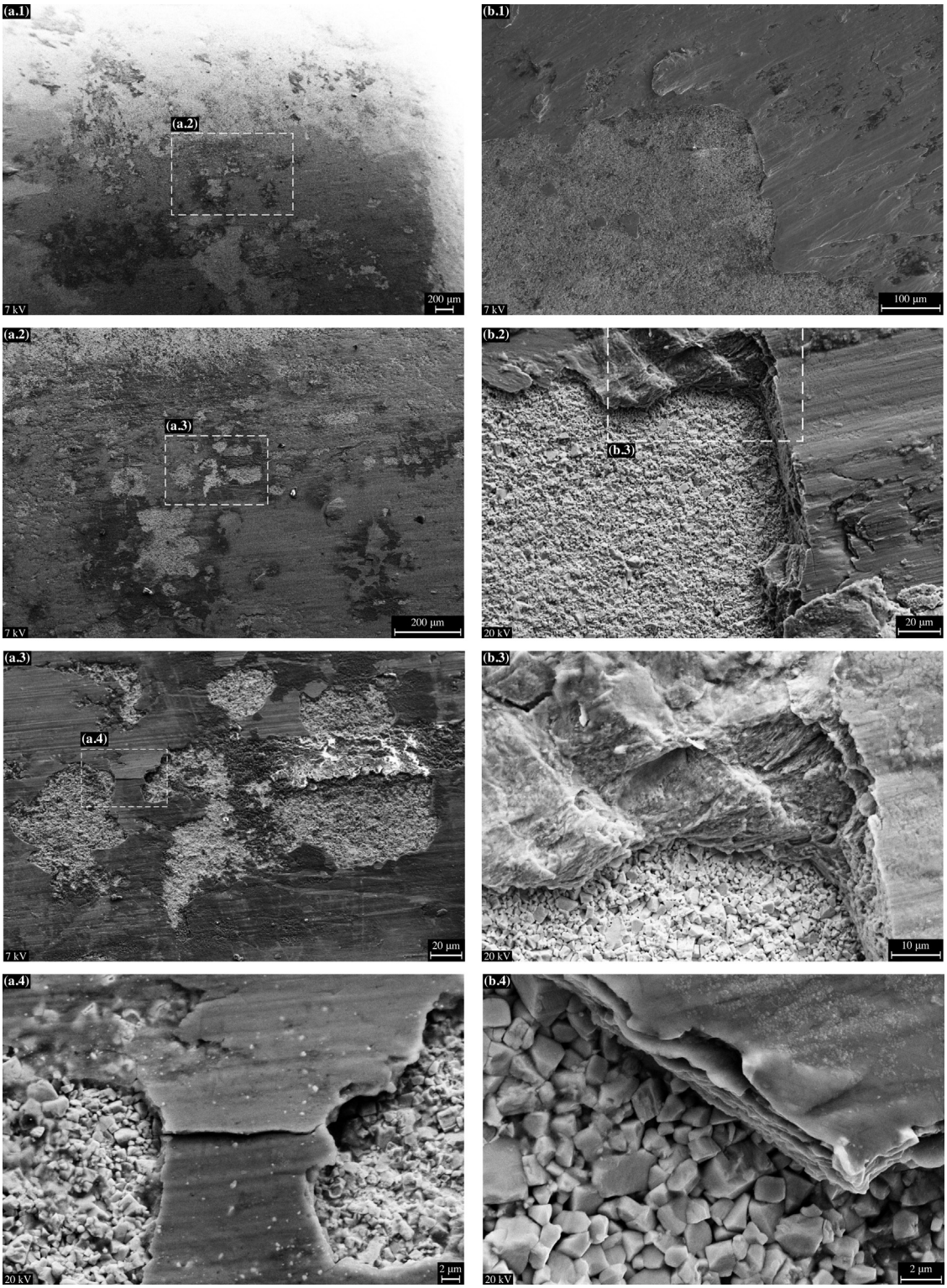

Fig. 14. SEM SE images of the rock tribofilm layer on peripheral insert in positions 1 at different magnifications. (a) Grade WC(4.4)–9.5NFCM. (b) Grade WC(3.9 n)–9.7Co. Electron accelerating voltage is given on each image.

5. Conclusions

Laboratory abrasion and full–scale drilling tests were performed with the aim of identifying the macro– and microscopic distinctive features and correlations of Cemented Carbide (CC) microstructure deterioration at different loading conditions and for different grade characteristics. Parameters analysed at the macro–scale are the volume or weight loss and the shape change, whereas scanning–electron microscope images of the worn specimens were examined to qualitatively characterize the wear behaviour of the grades at the micro–scale. Nine CC grades with different binder content, binder compositions, mean WC grains size and range of WC grains size distribution were studied.

Distinct pattern of zones of damaged microstructure surrounded by intact surface were found on the surfaces of the CC drill–bit inserts used in single impact tests. Damaged zones are non–uniformly scattered on

the surface of the CC insert varying from 20 to 250 μm in diameter. The pattern indicates the non–uniform nature of the contact due to the rock roughness and internal rock heterogeneities. Size of such insert–rock contact zones could be seen as a characteristic length–scale of the interaction and the behaviour of CC at this scale should be carefully considered when determining the overall response and wear of the insert.

Different wear traces were found in the full–scale drilling tests on the drill–bit inserts depending on their distance from the drill–bit axis. Inserts placed on periphery and being in contact with the borehole wall are predominantly worn form the side facing the wall. Wear traces on the inserts at the flat frontal plateau of the drill–bit are circular or elliptical in shape. The further from the drill–bit axis, the more wear traces are elongated along the drill–bit radial direction. The wear traces on all inserts are inclined towards the insert's leading edge, with respect to the direction of rotation. This can be explained by the harmful tensile forces present on the leading edge of the insert due to the sliding contact with rock.

The placement of CC inserts on the drill–bit crown was found to result in certain inserts being “protected” by the ones placed in front of them with respect to the direction of drill–bit rotation. The inserts in the leading position are more exposed to the intact rock and show significantly higher volume losses. In this light, placing inserts at different distances from the drill–bit rotation axis could result in a more evenly distributed workload.

Average volume losses in the full–scale drilling test show noticeable difference between the CC grades. The lowest volume losses were observed for the drill–bit equipped with the CC grade with narrow WC grains size distribution and pure cobalt binder. Higher wear rates were observed for the CC grades with normal WC grains size distribution and pure Cobalt binder, whereas lowest performance or highest wear rates were observed for the grades with others Ni–based binders.

Laboratory sliding abrasion (AV) and impact abrasion (LCPC) tests are unable to give results comparable to the full–scale drilling tests. Some parts of the overall wear behaviour are reproduced correctly, but the relative magnitudes of volume losses always differ from that measured in full–scale drilling tests. However, the AV test seems to be more accurate in predicting the relative CC grade volume losses, which can be explained by the similarity of the linear speed of the interaction with rock in AV and full–scale drilling tests. In order to achieve better prediction of wear behaviour with LCPC test the use of a rounded specimen geometry and lower rotation speed could be considered.

The appearance of the worn CC microstructure is not exactly reproduced in the laboratory tests, compared to that observed in the full–scale drilling test. The appearances differ by the amount of rock tribofilm on the surface and by the rounded versus angular shapes of WC grains. No signs of abrasive wear scratches were found after either of the tests, which confirms the non–abrasive nature of CC microstructure deterioration, when in contact with rock.

A specific pattern of rock tribofilm formation and removal was observed on the drill–bit's peripheral inserts in the full–scale drilling test. Non–uniformly scattered patches of naked CC surface 50–200 μm in diameter, surrounded by the rock tribofilm suggest the peeling–off mechanism of tribofilm removal. Undamaged appearance of those patches of naked CC zones suggests that portion of the CC microstructure fused with tribofilm also gets peeled off together with the later. Such mechanism of material removal could be expected on the surfaces with considerable adhered tribofilm layer.

The dominant micro–deterioration mechanisms typical for all different grades could not be identified. This study was limited to the analysis of only the exterior surfaces of the worn cemented carbide specimens. In perspective, an investigation of the state of the microstructure below the surface could bring useful information to determine the qualitative and even quantitative differences between deterioration mechanisms of CC grades.

Acknowledgment

This study is a part of the knowledge building research activities for industry funded by The Research Council of Norway (grant NFR 216436 and NFR 254984) and industrial consortia.

References

[1] W.A. Hustrulid, C. Fairhurst, A theoretical and experimental study of the percussive drilling of rock Part I - Theory of percussive drilling, Int. J. Rock. Mech. Min. Sci. 8 (1971) 311–333.
[2] S. Choudhary, Tungsten-carbide composite: a review, Int. J. Sci. Eng. Res. 3 (2012).
[3] I. Konyashin, B. Ries, Wear damage of cemented carbides with different combinations of WC mean grain size and Co content. Part II: laboratory performance tests on rock cutting and drilling, Int. J. Refract. Met. Hard Mater. 45 (2014) 230–237, http://dx.doi.org/10.1016/j.ijrmhm.2014.04.017.
[4] M.G. Gee, A. Gant, B. Roebuck, Wear mechanisms in abrasion and erosion of WC/Co and related hardmetals, Wear 263 (2007) 137–148, http://dx.doi.org/10.1016/j.wear.2006.12.046.
[5] I. Konyashin, B. Ries, Wear damage of cemented carbides with different combinations of WC mean grain size and Co content. Part I: astm wear tests, Int. J. Refract. Met. Hard Mater. 46 (2014) 12–19, http://dx.doi.org/10.1016/j.ijrmhm.2014.04.021.
[6] J. Angseryd, A. From, J. Wallin, S. Jacobson, S. Norgren, On a wear test for rock drill inserts, Wear 301 (2013) 109–115, http://dx.doi.org/10.1016/j.wear.2012.10.023.
[7] A.J. Gant, M.G. Gee, A.T. May, Microabrasion of WC-Co hardmetals in corrosive media, Wear 256 (2004) 954–962, http://dx.doi.org/10.1016/j.wear.2003.09.003.
[8] P.V. Krakhmalev, On the abrasion of ultrafine WC-Co hardmetals by small SiC abrasive, Tribol. Lett. 30 (2008) 35–39, http://dx.doi.org/10.1007/s11249-008-9309-2.
[9] S. Luyckx, N. Sacks, A. Love, Increasing the abrasion resistance without decreasing the toughness of WC–Co of a wide range of compositions and grain sizes, Int. J. Refract. Met. Hard Mater. 25 (2007) 57–61.
[10] B. Roebuck, M.G. Gee, Abrasion resistance of wide grained WC/Co hardmetals, in: EUROMET, Lausanne, 2002.
[11] B. Roebuck, A.J. Gant, M.G. Gee, Abrasion and toughness property maps for WC/Co hardmetals, Powder Metall. 50 (2007) 111–114, http://dx.doi.org/10.1179/174329007X211526.
[12] M.G. Gee, C. Phatak, R. Darling, Determination of wear mechanisms by stepwise erosion and stereological analysis, Wear 258 (2005) 412–425, http://dx.doi.org/10.1016/j.wear.2004.02.013.
[13] J. Heinrichs, M. Olsson, S. Jacobson, Surface degradation of cemented carbides in scratching contact with granite and diamond-The roles of microstructure and composition, Wear 342–343 (2015) 210–221, http://dx.doi.org/10.1016/j.wear.2015.08.024.
[14] J. Heinrichs, M. Olsson, S. Jacobson, Initial deformation and wear of cemented carbides in rock drilling as examined by a sliding wear test, Int. J. Refract. Met. Hard Mater. 64 (2017) 7–13, http://dx.doi.org/10.1016/j.ijrmhm.2016.12.011.
[15] U.S. Banda, Rock Mass Characterization of the Printzsko¨ld and Fabian Orebodies at the Malmberget Mine, 2008.
[16] R. Selmer-Olsen, R. Lien, Bergartens borbarhet og sprengbarhet, Tek. Ukebl. 34 (1960) 3–11.
[17] D. Tkalich, M. Fourmeau, A. Kane, C.C. Li, G. Cailletaud, Experimental and numerical study of Kuru granite under confined compression and indentation, Int. J. Rock. Mech. Min. Sci. 87 (2016) 55–68, http://dx.doi.org/10.1016/j.ijrmms.2016.05.012.
[18] F. Dahl, A. Bruland, P. Drevland, B. Nilsen, E. Grøv, Classifications of properties influencing the drillability of rocks, based on the NTNU / SINTEF test method, Tunn. Undergr. Sp. Technol. Inc. Trenchless Technol. Res. 28 (2012) 150–158, http://dx.doi.org/10.1016/j.tust.2011.10.006.
[19] F.R.N. Nabarro, S. Shrivastava, S.B. Luyckx, The size effect in microindentation, Philos. Mag. 86 (2006) 4173–4180.
[20] S. Shrivastava, S. Luyckx, Evidence and importance of an intrinsic length scale, in: Proceedings of the WC-Co, International Conference Sci. Hard Mater. ICSHM-9, Montego Bay, Jamaica 11–12, 2008.
[21] H. Conrad, Y.W. Shin, G.A. Sargent, N.R. Cousins, J.B. Clark, Specialty Steels and Hard Materials, 1983. http://dx.doi.org/10.1016/B978-0-08-029358-5.50028-8.
[22] K. Anand, H. Conrad, Local impact damage and erosion mechanisms in WC-6wt.%Co alloys, Mater. Sci. Eng. 105–106 (1988) 411–421, http://dx.doi.org/10.1016/0025-5416(88)90725-2.
[23] GOM system, ⟨http://www.gom.com/3d-software.html⟩, 2017.
[24] G.M. Hamilton, L.E. Godman, The stress field created by a circular sliding contact, J. Appl. Mech. (1966) 371–376, http://dx.doi.org/10.1115/1.3625051.
[25] D. Tkalich, G. Cailletaud, V.A. Yastrebov, A. Kane, Multiscale Modeling of Cemented Tungsten Carbide in Hard Rock Drilling, 2017. (Submitted for publication).
[26] K.J. Swick, G.W. Stachowiak, A.W. Batchelor, Mechanism of wear of rotary-percussive drilling bits and the effect of rock type on wear, Tribol. Int. 25 (1992) 83–88, http://dx.doi.org/10.1016/0301-679X(92)90125-7.
[27] F.P. Bowden, D. Tabor, F. Palmer, Frict. Lubr. Solids (1951), http://dx.doi.org/10.1119/1.1933017.
[28] C.D. Martin, N.A. Chandler, The progressive fracture of Lac du Bonnet granite, Int. J. Rock. Mech. Min. Sci. Geomech. Abstr. 31 (1994) 643–659.
[29] U. Beste, S. Jacobson, S. Hogmark, Rock penetration into cemented carbide drill buttons during rock drilling, Wear 264 (2008) 1142–1151, http://dx.doi.org/10.1016/j.wear.2007.01.029.
[30] S. Olovsjö, R. Johanson, F. Falsafi, U. Bexell, M. Olsson, Surface failure and wear of cemented carbide rock drill buttons-The importance of sample preparation and optimized microscopy settings, Wear 302 (2013) 1546–1554, http://dx.doi.org/10.1016/j.wear.2013.01.078.